Structural Engineering and Mechanics, *Vol. 57, No. 4 (2016) 681-701*
DOI: http://dx.doi.org/10.12989/sem.2016.57.4.681

Seismic behavior of T-shaped steel reinforced high strength concrete short-limb shear walls under low cyclic reversed loading

Zongping Chen[*1,2], Jinjun Xu[**1], Yuliang Chen[1] and Yisheng Su[1]

[1]*College of Civil Engineering and Architecture, Guangxi University, Nanning, 530004, P.R. China*
[2]*Key Laboratory of Disaster Prevention and Structural Safety of Chinese Education Ministry, Guangxi University, Nanning, 530004, P.R. China*

(Received February 24, 2015, Revised December 16, 2015, Accepted January 15, 2016)

Abstract. This paper presents an experimental study of six steel reinforced high strength concrete T-shaped short-limb shear walls configured with T-shaped steel truss under low cyclic reversed loading. Considering different categories of ratios of wall limb height to thickness, shear/span ratios, axial compression ratios and stirrup reinforcement ratios were selected to investigate the seismic behavior (strength, stiffness, energy dissipation capacity, ductility and deformation characteristics) of all the specimens. Two different failure modes were observed during the tests, including the flexural-shear failure for specimens with large shear/span ratio and the shear-diagonal compressive failure for specimens with small shear/span ratio. On the basis of requirement of Chinese seismic code, the deformation performance for all the specimens could not meet the level of 'three' fortification goals. Recommendations for improving the structural deformation capacity of T-shaped steel reinforced high strength concrete short-limb shear wall were proposed. Based on the experimental observations, the mechanical analysis models for concrete cracking strength and shear strength were derived using the equivalence principle and superposition theory, respectively. As a result, the proposed method in this paper was verified by the test results, and the experimental results agreed well with the proposed model.

Keywords: steel reinforced concrete (SRC); high strength concrete; short-limb shear wall; T-shaped wall; seismic behavior; deformation; cracking strength; shear strength

1. Introduction

In recent years, with the constantly expanding scales of residential construction and vigorously promoting the modernization of housing industry, multi-layer and high-rise buildings in China are generally welcomed by customers, and they can effectively take advantage of limited land resources to improve human lives and living conditions. In earthquake zones, reinforced concrete (RC) shear walls are the common lateral load resisting systems for their good shear capacity and deformation performance (Mullapudi *et al*. 2013, Mosoarca 2014, Su and Wong 2007, Gonzales

∗Corresponding author, Ph.D., E-mail: zpchen@gxu.edu.cn
**Corresponding author, Ph.D. Student, E-mail: jjxu_concrete@163.com

http://www.techno-press.org/?journal=sem&subpage=8 ISSN: 1225-4568 (Print), 1598-6217 (Online)

and López-Almansa 2012, Quiroz *et al*. 20113, Jalali and Dashti 2010). However, the building development must be adapted to the society demand, which means that people demand higher requirements on the flexibility of using space and comfortable sensation as well as concern about the structural safety. Thus, to meet the requirements for architectural functions such as light, space, appearance, and to consider the furniture arrangement with non-exposed beams and columns, a new structural form named short-limb (or leg) shear wall was put into use based on the structural foundation of shear walls and special shaped columns (Rong 1997, Dai 2013). Compared with the normal shear wall, the short-limb shear wall refers to the wall with limb height to thickness ratio h/b (h is the wall limb height, b is the wall thickness) of 5 to 8 according to the Chinese code JGJ3-2010 (2011), where the wall thickness of this component is greater than or equal to 200 mm, and its height ranges from 1000 mm to 2500 mm. Actually, the short-limb shear wall is a kind of derivatives of special shaped column, hence, the L-shaped, T-shaped, ┼-shaped, Z-shaped or even line-shaped (occasionally used) cross sections are adopted for this type of shear walls (Ding and Zhu 2012).

RC short-limb shear wall has been investigated experimentally and numerically. Xue (2005), Zhang *et al*. (2011) conducted elastic-plastic analysis on T-shaped, line-shaped and ┼-shaped RC short-limb shear walls using ANSYS software, and the calculation results showed that the ductility and the ability of the energy dissipation of these shear walls were not good when the limb height to thickness ratio is 0.6. Brueggen (2009), Li and Li (2012) conducted series of tests on the seismic behavior of RC short-limb shear walls. The performance indexes of these components investigated were not suitable for tall and super-tall buildings. Hence, it is similar to the RC normal shear walls with low bearing capacity and poor seismic performance due to the limitation of RC materials. In order to overcome the above mentioned deficiencies, the focuses on the concrete strength and reinforcement ratio are the main ways to improve the bearing capacity and seismic behavior of vertical bearing members.

With the development of architectural structural system, the steel-concrete (S-C) composite structures start to show their stronger performance and better economic advantages compared with the RC structures. Liao *et al*. (2012) reported an investigation into the behavior of RC shear walls by implanting steel reinforced concrete (SRC) boundary columns. Qian *et al*. (2012) proposed an innovative composite shear wall, named steel tube-reinforced concrete (STRC) composite wall, with steel tubes embedded at the wall boundary elements and fully anchored within the foundation. In addition, the concrete or reinforced concrete encased with or filled in steel plates is an excellent combination form to enhance the mechanical behavior of concrete shear walls. Based on the before-mentioned idea, Yamada (1992), Nie *et al*. (2013), Meftah *et al*. (2007), Altin *et al*. (2013) conducted a series of tests to study the shear capacity and seismic response of steel encased concrete shear walls. Hence, it is undoubtedly logically that S-C composite short-limb shear walls can replace the RC short-limb shear walls in seismic zones. For this purpose, a series of testes were conducted by many researchers (e.g., Xie 2008, Yu 2009, Li 2010, Wang 2008, Yang *et al*. 2009), and many design methods for shear capacity were put forward.

Moreover, there are also many methods to enhance the concrete strength in RC shear walls, such as utilizing high strength concrete, forming confined concrete and strengthening reinforced concrete with CFRP (Lao and Han 2011, Zhou *et al*. 2013). Combining with the high strength concrete and steel reinforced concrete to form a new kind of short-limb shear wall structural system, named steel reinforced high strength concrete (SRHSC) short-limb shear walls, can yet be regarded as an effective strengthening measure in high-rise buildings.

In this paper, six steel reinforced high strength concrete T-shaped short-limb shear walls were

tested under low cyclic reversed loading. On the basis of test parameters, the load-displacement hysteretic relationships, strength, stiffness, energy dissipation capacity, ductility and deformation characteristics of all the specimens were discussed. In addition, the measures for improving the structural deformation capacity of SRHSC short-limb shear walls are proposed. Based on the experimental observations, the mechanical analytical models for concrete cracking strength and shear strength are derived using the equivalence principle and superposition theory, respectively.

2. Experimental program

2.1 Specimen characteristics

Six specimens with different parameters were designed and tested in this study. The primary parameters were the ratio of wall limb height to thickness, shear/span ratio ($\lambda=H/h$, H is the length of shear wall, h is the wall limb height), axial compression ratio ($n=N/(f_cA)$, N is the axial compressive force, f_c is the axial compressive strength of concrete, A is the wall cross-sectional area) and stirrup reinforcement ratio (ρ_{sv}). In considerations of the available maximum loading capacity of the actuator and the conditions of the laboratory, the scale ratio of the specimens was finally set to 1:3. The detailed dimensions of the specimens are illustrated in Fig. 1 and listed in Table 1. The built-in shape steel in the wall cross section is the steel truss shown in Fig. 2, in which the welded T-shaped steels in the T-shaped wall cross section ends were connected (in fact, using the way of welding) by crossed diagonal steel flats (also named web members) and

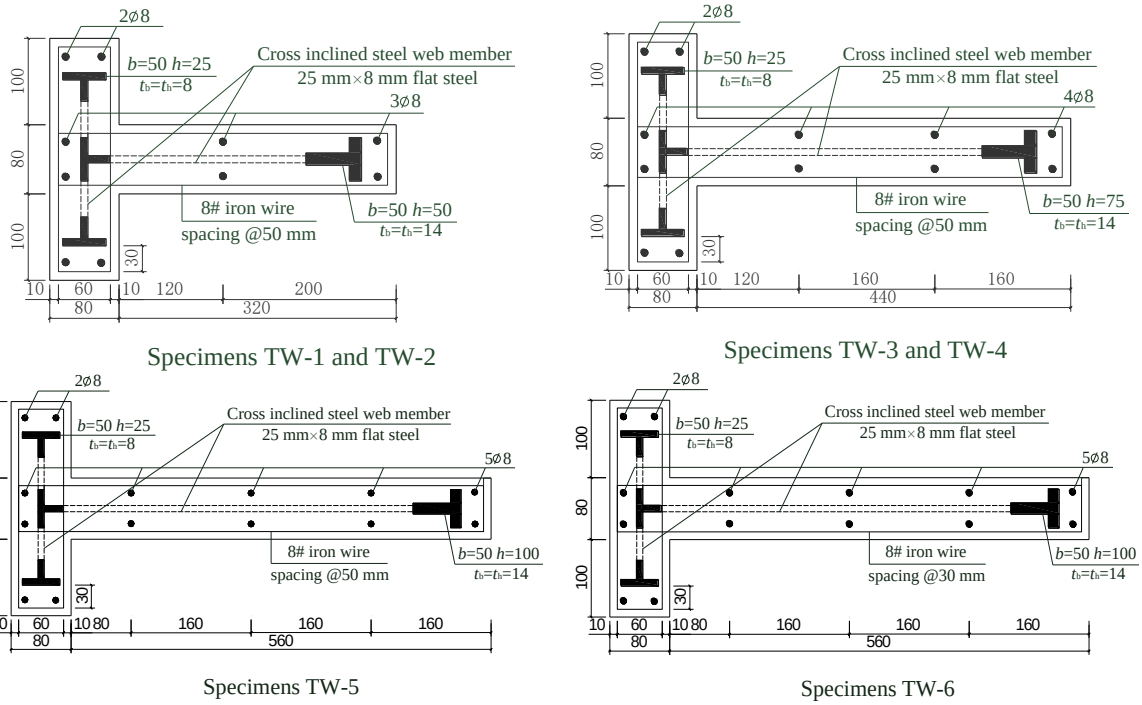

Fig. 1 Detailed parameters of specimens

Table 1 Design parameters of specimens

Code	h/b	λ	H (mm)	n	s_w (mm)	ρ_{sv} (%)	f_{cu} (MPa)
TW-1	5.0	2.0	800	0.2	270	0.846 (@50)	76.0
TW-2	5.0	1.5	600	0.2	300	0.846 (@50)	84.4
TW-3	6.5	1.5	780	0.2	260	0.846 (@50)	80.8
TW-4	6.5	1.5	780	0.3	260	0.846 (@50)	82.4
TW-5	8.0	1.5	960	0.2	240	0.779 (@50)	80.0
TW-6	8.0	1.5	960	0.2	240	1.286 (@30)	81.4

Note: s_w is the spacing of two horizontal steel flats up and down; h/b is the wall limb height to thickness ratio.

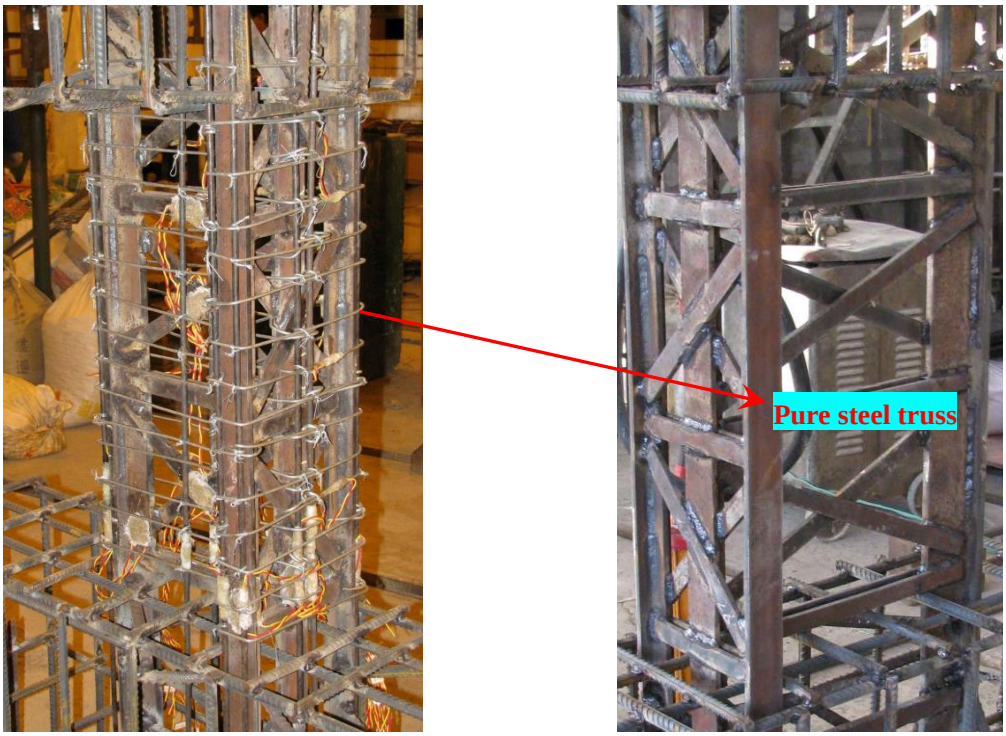

Fig. 2 Sketch of steel truss skeleton

horizontal steel flats. The wall limb cross-sectional thicknesses of all the specimens were the same, but three kinds of wall limb heights were fabricated to investigate the effect of wall limb height to thickness ratio on the seismic action of short-limb shear walls, including 400 mm, 520 mm and 640 mm. Through controlling of single test factor, the length of TW-1 is 1.5 times larger than that of TW-2 so that different failure modes may be produced in the tests, and the main focus is the shear/span ratio. In a similar way, the effect of axial compression ratio and the influence of stirrup reinforcement ratio (exploring the constraint mechanism) can be designed to comparatively study the seismic behavior of TW-3 and TW-4, TW-5 and TW-6, respectively. As shown in Fig. 3, the T-shaped cross section of shear wall was divided into 8 parts, ranging from *A* to *H*.

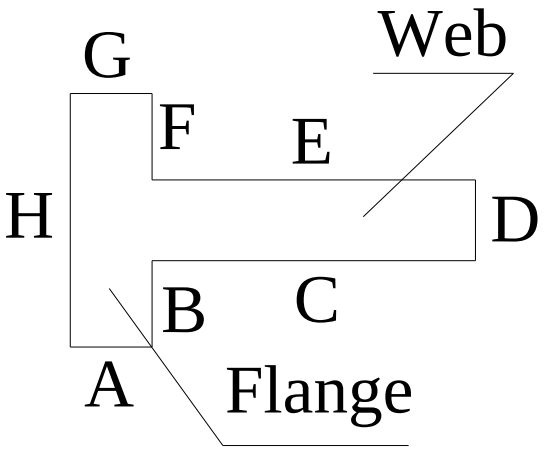

Fig. 3 Division of T-shaped cross section

Table 2 Mechanical prosperities of steels and reinforcement materials (mean values)

Steel type	Component	Yield strength f_y (MPa)	Ultimate strength f_u (MPa)	Elasticity modulus E_s (MPa)
Steel plate	8 mm thickness	314	458	1.855×10^5
	14 mm thickness	282	434	2.073×10^5
Reinforcement bar	HPB235(Φ8)	362	539	2.427×10^5
	No. 8 iron wire (Φ4)	342	428	-

2.2 Material properties

The mechanical properties of steels and reinforcement materials obtained from the material property tests are listed in Table 2. The average cubic compressive strengths of the specimen concrete f_{cu} (the length of the standard cubic concrete sample is 150 mm) obtained on the same time of testing the shear walls are 76.0 MPa for TW-1, 84.4 MPa for TW-2, 80.8 MPa for TW-3, 82.4 MPa for TW-4, 80.0 MPa for TW-5 and 81.4 MPa for TW-6.

2.3 Test setup and loading sequences

The testing system shown in Fig. 4 consisted of a 1000 kN servo-controlled hydraulic actuator to generate the cyclic horizontal load and a 1000 kN hydraulic jack for application of the constant vertical load. The loading direction for specimens illustrated in Fig. 5 is along the wall web. In the presence of the hinge connection, the top of the specimen could rotate freely and only the shear force and the axial force could be transferred to the specimen, thereby the free end boundary condition was satisfied. The horizontal actuator and the vertical jack were connected to the sliding devices at the top end without rotation. However, the specimen at the bottom end was fixed in order to generate the bending moment.

In the test, the vertical load was applied to the specimen and then maintained constant. Horizontal force was imposed using the force-control scheme repeated only once at each control

point before the specimen yields, and then using the displacement-control scheme repeated three times at each control point after the specimen yields. The loading history included elastic cycles and inelastic cycles. The elastic cycles were conducted under load control at load levels of 0.3 p_y, 0.7 p_y, and 1.0 p_y. One cycle was imposed at each of the lateral load levels of 0.3 p_y, 0.7 p_y. The inelastic levels were taken to lateral displacement levels of Δ_y, $1.0\Delta_y$, $2.0\Delta_y$, $3.0\Delta_y$, $4\Delta_y$, …. Three cycles were imposed at each displacement level. The test was completed until the lateral load resistance decreased below 85% of the maximum measured lateral load capacity of the specimen. The lateral displacement applied to the top of the specimen was varied as shown in Fig. 6.

2.4 Instrumentation

Loads and displacements at critical locations were measured for all the specimens, as shown in Fig. 4. Two displacement meters were mounted to a rigid steel reference frame to measure lateral displacements: the top one (DM1 sketched in Fig. 4) was fixed at the same height of the loading point and the bottom one (DM1 sketched in Fig. 4) was fixed on the foundation support of specimen. Furthermore, another two displacement meters (DM3 and DM4 sketched in Fig. 4) were mounted vertically along the length of each wall so that the deformation of the wall base could be determined.

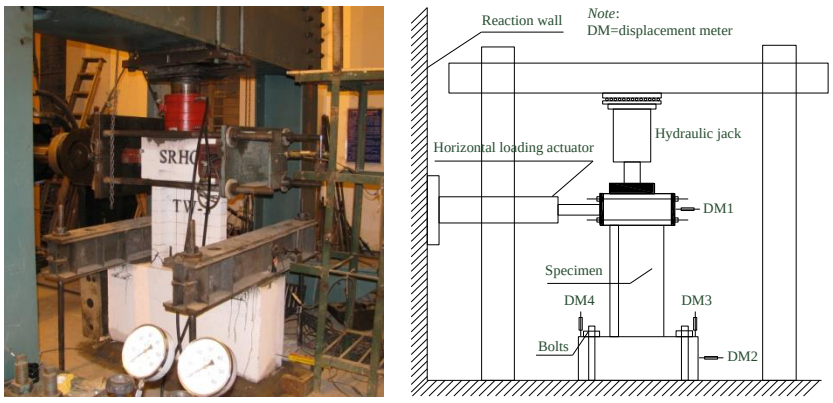

Fig. 4 Test setup

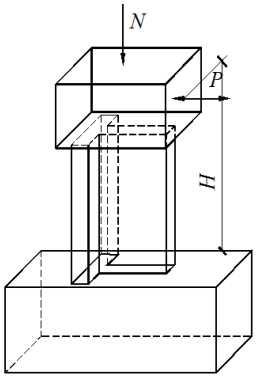

Fig. 5 Loading direction

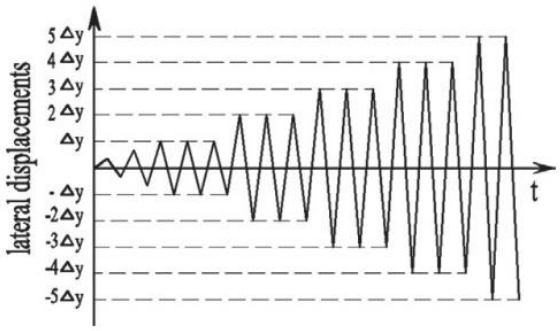

Fig. 6 Loading pattern

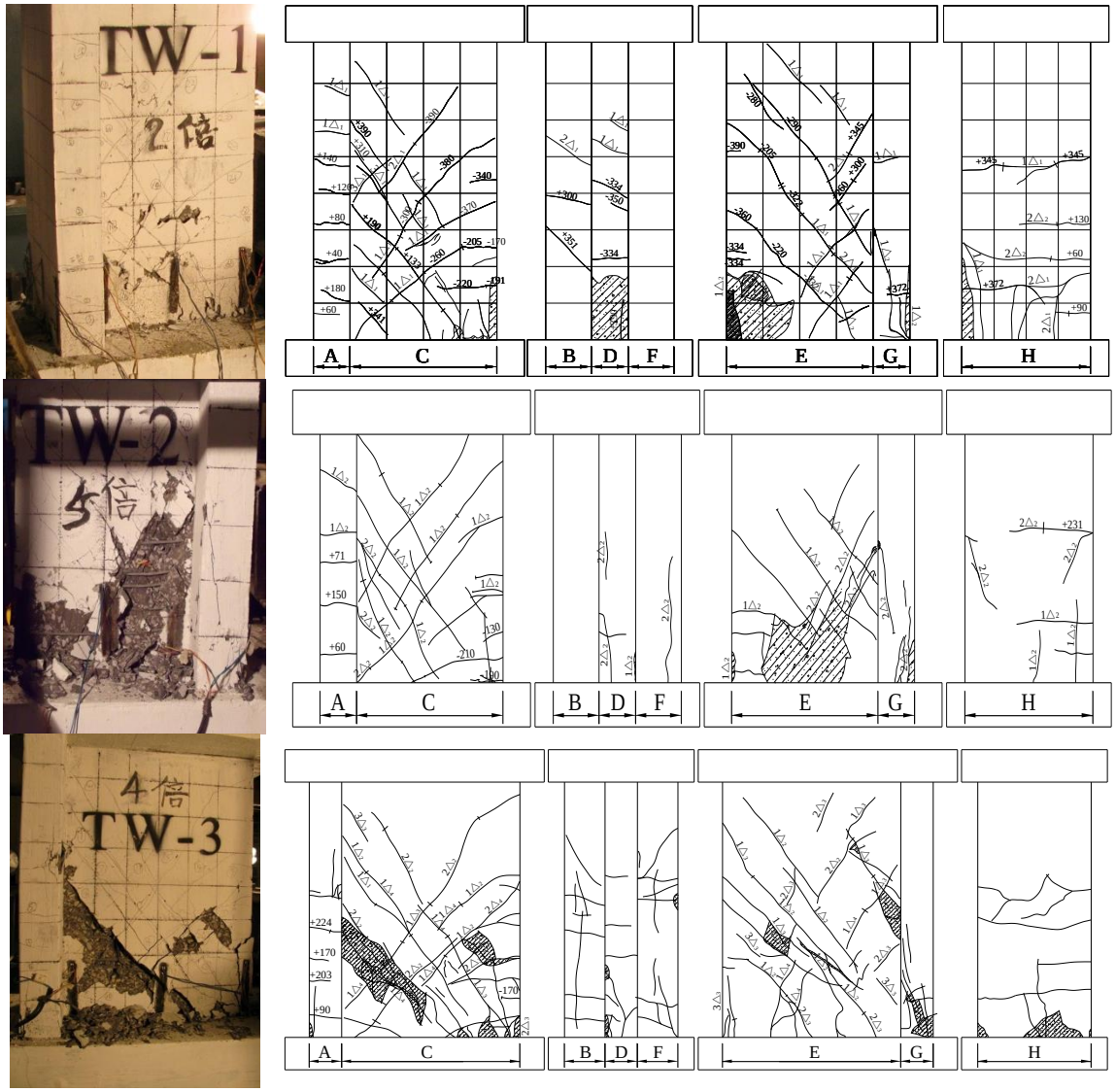

Fig. 7 Failure pattern of specimens

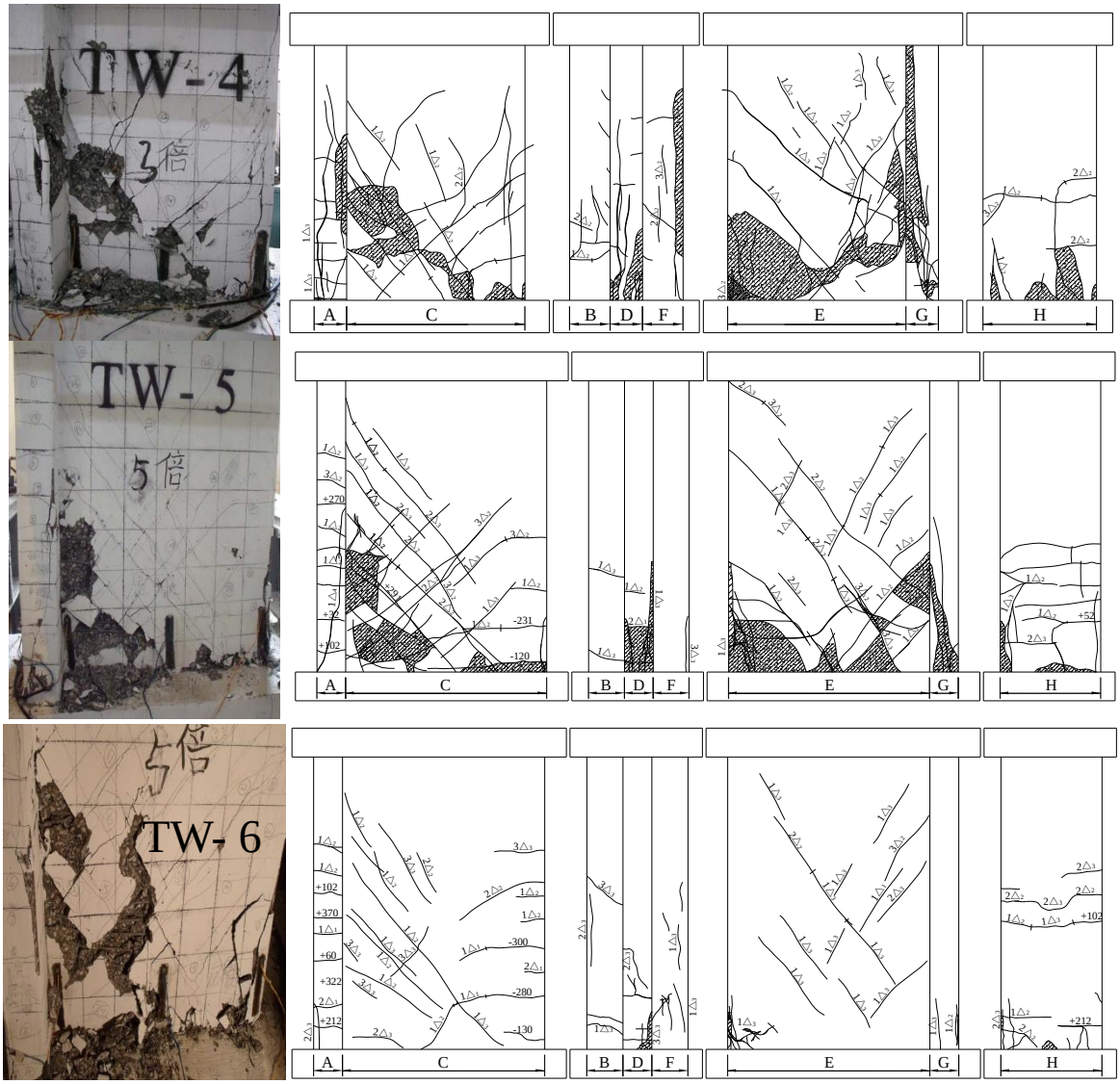

Fig. 7 Continued

3. Test results and discussion

3.1 Failure modes

3.1.1 Flexural-shear failure

One specimen exhibited flexural-shear failure mode during the test, the specimen TW-1. In the force-control loading stage, when the lateral force reached positive 50 kN, several horizontal cracks appear at the root of wall flange. Then the opposite loading to negative 200 kN resulted in several horizontal cracks distributing at the root of wall web. With the increasing of loads, some diagonal cracks developed from the original horizontal cracks, and when the lateral force reached

about 300 kN, the densely distributed crossed diagonal cracks formed along the wall length upward, and at the same time, the specimen yielded accordingly. In the displacement-control loading stage after the specimen was yielded, the horizontal cracks developed into a few of main cracks throughout the wall root, and when the applied displacement firstly reached positive 9 mm and negative 11 mm, the concrete at the web began to crush with dividing the wall surface into a number of diamond-shaped pieces. After that, the area of the crushing concrete is gradually expanding with the increasing of the displacement amplitude. The final failure mode of TW-1 is shown in Fig. 7.

3.1.2 Shear-diagonal compressive failure

Since the rest of the specimens demonstrated similar phenomenon during the tests, only the specimen TW-2 is discussed here. In the force-control loading stage, similar horizontal and diagonal cracking patterns as TW-1 are formed at the root of wall web and flange. However, in the displacement-control loading stage after the specimen yielded, no evident horizontal crack development along the wall length could be observed. When the applied displacement reaches 7 mm, the test phenomenon is similar to TW-1. The shear-diagonal compressive failure is the main failure mode, as illustrated in Fig. 7.

3.2 Hysteretic responses and load-displacement curves

The load-displacement hysteretic and skeleton curves of all the specimens are shown in Fig. 8 and Fig. 9, respectively. The hysteretic loops of all the specimens are pinched, indicating that the seismic behavior of T-shaped SRHSC short-limb shear wall is poor. Based on effect of the shear span ratio, the curves of the TW-1 demonstrated lower loading capacity but higher energy dissipation capacity than those of the TW-2, and it reflected the failure mechanisms of the specimens according to the test failure phenomenon. For the effect of axial compression ratio, the positive peak loading capacities between TW-3 and TW-4 were almost unanimous, however, the

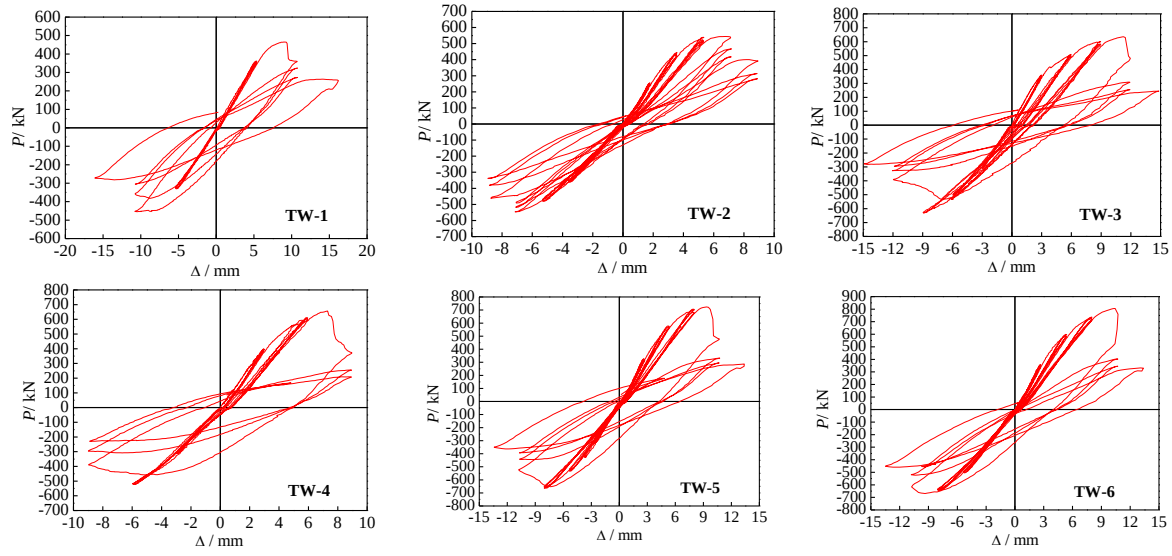

Fig. 8 Hysteretic curves

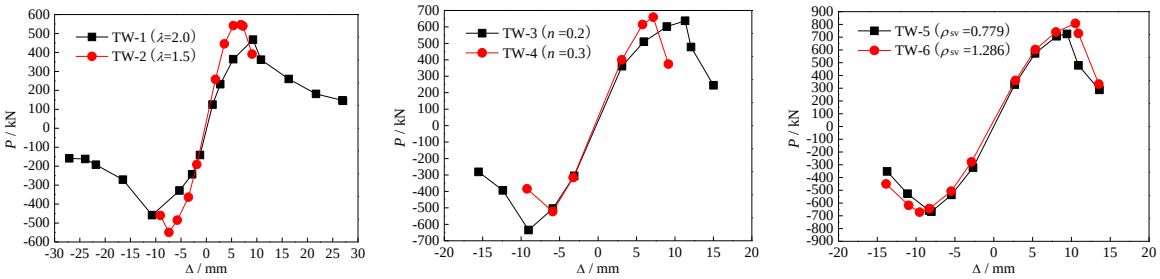

Fig. 9 Skeleton curves

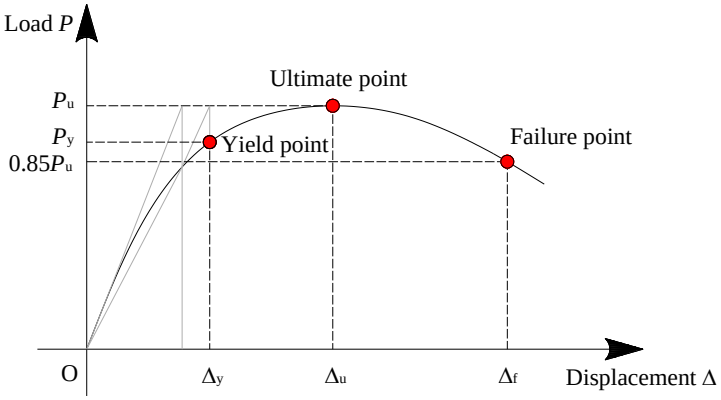

Fig. 10 Characteristic points on load-displacement curve

Table 3 Summary of measured results

Code		TW-1	TW-2	TW-3	TW-4	TW-5	TW-6
P_y /kN	Positive	295.44	412.91	448.09	633.96	634.50	596.73
	Negative	302.64	369.81	248.06	396.23	496.86	457.29
Δ_y /mm	Positive	4.36	3.82	4.62	6.58	6.28	5.37
	Negative	3.43	3.73	2.47	3.86	4.79	4.69
P_u /kN	Positive	467.06	546.3	637.2	659.0	725.2	808.3
	Negative	458.82	549.4	634.4	524.3	667.6	671.5
Δ_u /mm	Positive	9.25	6.85	11.33	7.18	9.44	10.52
	Negative	10.73	7.38	9.04	6.04	8.04	9.55
P_f /kN	Positive	397.00	464.34	541.65	560.12	616.45	687.01
	Negative	390.00	466.98	539.21	445.61	567.43	570.75
Δ_f /mm	Positive	10.31	8.34	11.78	8.10	10.19	11.18
	Negative	13.31	8.99	10.36	8.37	10.37	11.78

negative peak loading capacity of TW-3 subjected to lower axial force was larger than that of TW-4 with a higher axial force level. In addition, the curves of TW-6 illustrated higher loading capacity and stiffness than those of TW-5, indicating that the cyclic behavior of subassemblies with high stirrup reinforcement ratio is superior to those with low stirrup reinforcement ratio.

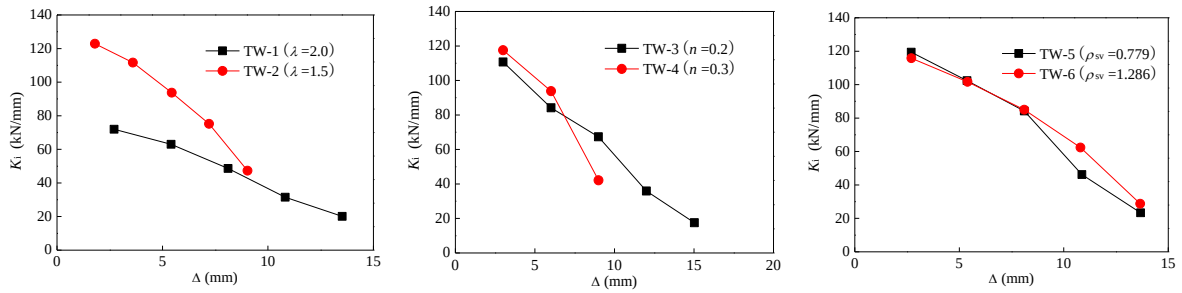

Fig. 11 Stiffness degradation

As shown in Fig. 10, three critical characteristic points, namely, yield point (P_y, Δ_y), ultimate point (P_u, Δ_u) and failure point (P_f, Δ_f) can be obtained from the skeleton curves, and the characteristic loads and displacements corresponding to these three points are listed in Table 3. The yield point can be determined using the graphical method in Tao *et al*. (2013) as shown in Fig. 10. The ultimate load P_u is selected as the maximum load, and the failure displacement Δ_f is defined as the maximum displacement corresponding to the load no less than $0.85P_u$.

3.3 Stiffness degradation

The secant stiffness K_i is used to describe the stiffness degradation of the specimens as shown in Fig. 11, and the formula for calculating K_i can be found in Lao and Han (2011).

$$K_i = \left(\left|+P_{ji}\right| + \left|-P_{ji}\right|\right) \Big/ \left(\left|+\Delta_{ji}\right| + \left|-\Delta_{ji}\right|\right) \tag{1}$$

Where P_{ji} and Δ_{ji} is the maximum values of the load and the corresponding displacement under the ith cycle when the deformation is controlled as $\Delta_j = j \times \Delta_y$.

It can be clearly seen from Fig. 11 that the secant stiffness of all the specimens degrades evidently during the entire loading process. The stiffness of the specimen TW-2 (λ=1.5) with shear-diagonal compressive failure is much higher than that of the specimen TW-1 (λ=2.0) with flexural-shear failure, indicating that the shear span ratio plays a vital role in the seismic behavior of T-shaped SRHSC short-limb shear walls. There is also a remarkable effect of axial compression ratio on the secant stiffness of specimens, and it is showed that before the specimens yield, the stiffness of TW-4 (n=0.3) is slightly larger than that of TW-3 (n=0.2), while after the specimens yield, the stiffness of TW-4 is smaller than that of TW-3. It means that the higher axial force is beneficial to increase the initial elastic lateral stiffness of short-limb shear wall member, however, an increase of the axial compression ratio can lead to a decrease of the elastic-plastic lateral stiffness of short-limb shear wall member due to the wide range of seismic damage and failure. In addition, the effect of stirrup reinforcement ratio on the secant stiffness of specimens illustrates that there is no significant difference between the TW-5 and TW-6 in the early stage of loading, however, with the increasing of displacement amplitude, the stiffness of TW-6 with large stirrup reinforcement ratio is much higher than that of TW-5 with small stirrup reinforcement ratio, indicating that an increase of lateral constraint can enhance the elastic-plastic lateral stiffness for the short-limb shear wall.

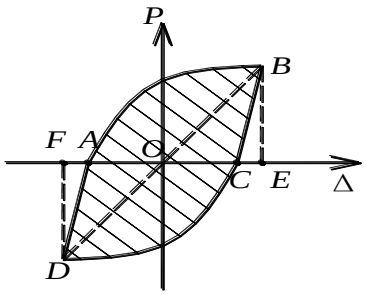

Fig. 12 Energy dissipation capacity calculation diagram

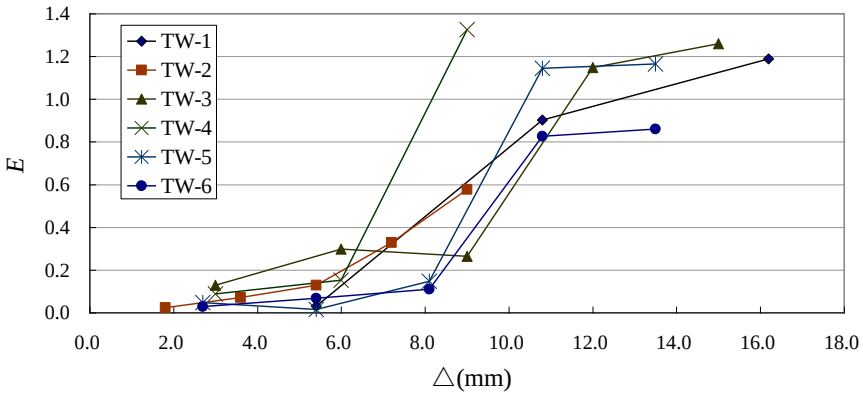

Fig. 13 Energy dissipation capacity of specimens

3.4 Energy dissipation capacity

In order to evaluate the accurate energy dissipation ability of all the specimens, the energy dissipation coefficient E is calculated by Eq. (2), where $S_{(ABC+CDA)}$ and $S_{(OBE+ODF)}$ are the areas of the shadow as shown in Fig. 12.

$$E = \frac{S_{(ABC+CDA)}}{S_{(OBE+ODF)}} \tag{2}$$

Fig. 13 illustrates the energy dissipation coefficient of all the specimens during the whole process of loading. It can be seen that the energy dissipations are steadily and evidently enhanced with the increasing of the cyclic numbers after the specimens yield. The effects of ratio of wall limb height to thickness, shear/span ratio, axial compression ratio and stirrup reinforcement ratio on the energy dissipation capacity of T-shaped SRHSC short-limb shear walls can be explained via the final E value as follows: 1) the specimens TW-3 and TW-4 with wall limb height to thickness ratio of 6.5 have the larger cumulative E than the specimens with wall limb height to thickness ratios of 5 and 8, and it can be explained that when the wall limb height to thickness ratios is 5 and 8, the short-limb shear walls are transformed into the special shaped column and the normal shear wall, respectively, so that the failure mechanism can be changed accordingly; 2) the specimen TW-1 (λ=2.0) with flexural-shear failure demonstrates better energy dissipation capacity than that

of the specimen TW-2 (λ=1.5) with shear-diagonal compressive failure; 3) the specimen TW-4 subjected to larger axial force (n =0.3) illustrates larger energy dissipation capacity than that of the specimen TW-3 under smaller axial compression ratio (n =0.2), and the reason may be ascribed to the increasing of internal energy consumption of T-shaped SRHSC short-limb shear walls with a higher axial force level due to the sufficient destruction of composite materials; 4) the specimen TW-5 with a lower stirrup reinforcement ratio shows larger cumulative E than that of the specimen TW-6 with a higher stirrup reinforcement ratio, indicating that the destruction of specimen with weak constraint is more serious than that of the specimen with strong constraint.

3.5 Deformation performance

3.5.1 Ductility

Ductility plays a critical role in the seismic design of SRC structures. The displacement ductility ratio can be expressed as $\mu=\Delta_f/\Delta_y$. The mean displacement ductility ratios of all the specimens listed in Table 4 are largely less than 3.0, indicating that the ductility of T-shaped SRHSC short-limb shear walls is not good enough.

Fig. 14(a) shows the effect of ratio of wall limb height to thickness on μ(s) of all the specimens. It can be observed that an increase of wall limb height to thickness ratio leads to significant reduction of μ, showing that controlling the wall limb height to thickness ratio within a reasonable range is very important in seismic zones.

The relationship between μ and λ is shown in Fig. 14(b). A trend can be found that the displacement ductility ratio of TW-1 with large shear/span ratio is higher than that of TW-2 with small large shear/span ratio, indicating that the deformation capacity of the specimen with flexural-shear failure is superior to that of the specimen with shear-diagonal compressive failure.

The relationship between μ and n for T-shaped SRHSC short-limb shear walls is shown in Fig. 14(c). It can be obviously seen that an increase of axial compression ratio leads to a decrease of displacement ductility ratio, indicating that the specimens subjected to high axial force reduce the lateral deformation under the action of horizontal load.

In addition, the effect of stirrup reinforcement ratio on μ(s) between TW-5 and TW-6 are illustrated in Fig. 14(d). It can be clearly found that an increase of stirrup reinforcement ratio leads to an increase of displacement ductility ratio. The reason can be explained that the high strength

Table 4 Performance indexes of SRHSC short-limb shear walls in the test

Code	Mean μ	Good use		Ensuring the personal safety		Preventing the collapse	
		Δ_1 (mm)	θ_1	Δ_2 (mm)	θ_2	Δ_3 (mm)	θ_3
TW-1	3.12	1.55	1/905	9.24	1/87	9.30	1/78
TW-2	2.30	1.20	1/896	7.11	1/84	7.94	1/77
TW-3	3.37	1.60	1/848	9.34	1/84	9.45	1/75
TW-4	1.70	2.26	1/524	6.75	1/117	7.10	1/111
TW-5	1.89	1.21	1/1406	8.73	1/111	9.95	1/97
TW-6	2.30	1.34	1/1486	9.98	1/96	10.31	1/94

Note: Δ_1, Δ_2 and Δ_3 are the horizontal displacements of the first level, the second level and the third level, respectively; θ_1, θ_2 and θ_3 are the interlayer displacement angles corresponding to Δ_1, Δ_2 and Δ_3, respectively.

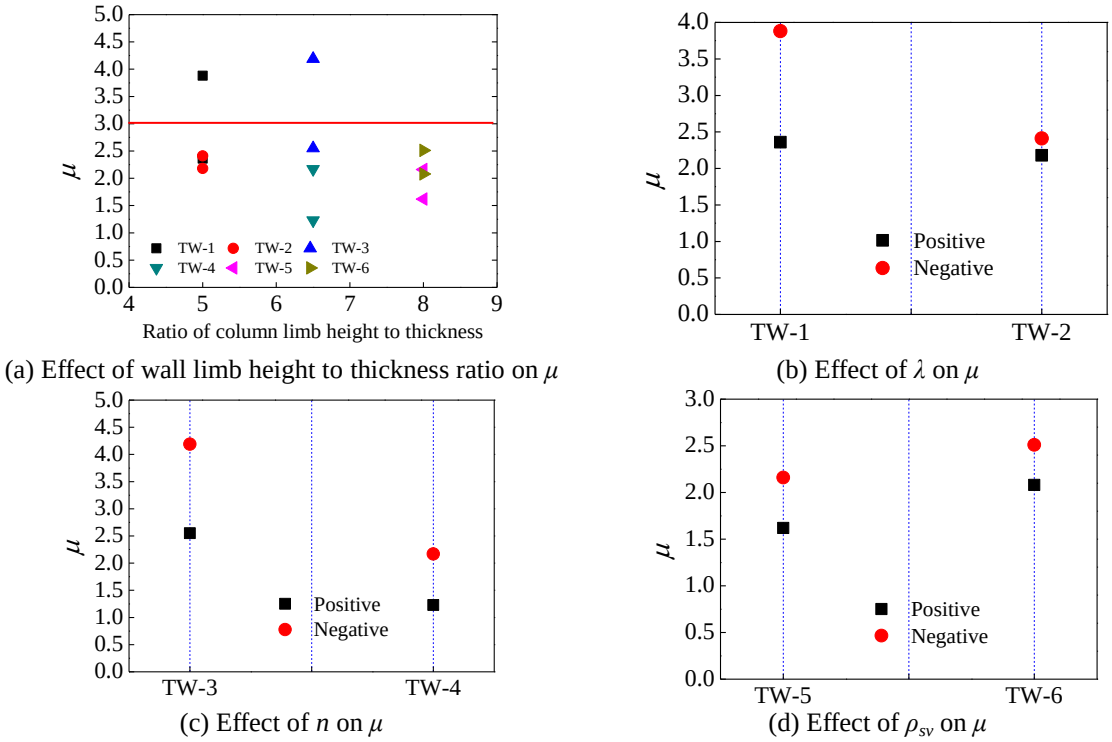

(a) Effect of wall limb height to thickness ratio on μ

(b) Effect of λ on μ

(c) Effect of n on μ

(d) Effect of ρ_{sv} on μ

Fig. 14 Relationships between test parameters and displacement ductility ratios

concrete in the reinforcement cage skeleton can be effective constrained by means of configuring with horizontal reinforcement stirrup, and furthermore, there is a positive correlation relationship between constraint level and stirrup reinforcement ratio. As a matter of fact, a good degree of constraint has a great contribution to the deformation capacity of a structural component. Therefore, the ductility of T-shaped SRHSC short-limb shear walls can be enhanced with configuring with serried stirrups.

3.5.2 Interlayer displacement angle and discussion

Under the action of horizontal load, the increasing of structural deformation will develop the structural plasticity and grow the damage degree. Deformation capacity between the layers is one of the most significant indexes to evaluate the seismic performance of a structure. The interlayer displacement angle θ can be calculated as the ratio of horizontal displacement Δ to the length of shear wall H. Under the stipulation of current Chinese seismic code (GB50011-2010), three levels of fortification goals based on the theory of performance design are stipulated to control the structural safety and economy by using the interlayer displacement angle index, including the good use, ensuring the personal safety and preventing the collapse. Accordingly, the first level is defined as the state of appearing the first obvious crack, the second level is determined by the local concrete spalling off from the specimen after the specimen yields, while for the third level, it can be described that obvious wide cracks are cut through and a large number of concrete blocks are crushed and dropping from the specimen.

Table 4 lists the characteristic interlayer displacement angles of all the specimens. Apparently,

it can be observed that the interlayer displacement angles for three performance levels are 1/1486~1/524, 1/117~1/84 and 1/111~1/75, respectively; and their average interlayer displacement angles are 1/1011, 1/97 and 1/88, respectively. In spite of the extensive researches of normal RC shear walls in the literature, the topics on the seismic performance and performance indexes of SRHSC short-limb shear walls still have not been fully addressed since all the shear walls concerned in previous studies are either regular shape and large wall limb height to thickness ratio or configured with solid-web steel and normal concrete. Therefore, it is necessary to make clear the difference of performance level indexes between SRHSC short-limb shear wall and steel-normal strength concrete short-limb shear wall (SNSCSLSW) to achieve the performance-based design goal for SRHSC short-limb shear wall structures.

Table 5 shows the deformation performance indexes of SNSCSLSW specimens originated from (Xie 2008, Yu 2009, Li 2010, Wang 2008, Yang *et al*. 2009). It can be clearly seen that for the specimens from literature, the interlayer displacement angles for three performance levels are 1/1250~1/332, 1/136~1/21 and 1/73~1/16, respectively; and their average interlayer displacement angles are 1/850, 1/71 and 1/47, respectively. As shown from the comparison, the interlayer displacement angles of T-shaped SRHSC short-limb shear walls under different levels of performance are less than those of SNSCSLSW, indicating that the deformability of T-shaped SRHSC short-limb shear walls under seismic action is inferior to that of the SNSCSLSW. The reason is that the brittle nature of high strength concrete and the irregularity of cross section weaken the seismic behavior of T-shaped SRHSC short-limb shear walls, so that measures need to be put forward to improve the deformation performance of these components. Among the measures available in the literature, setting constraints at the end of component limb, increasing stirrup ratio in the cross section, setting oblique supports and optimizing steel configuration form are the common and effective ways to enhance the seismic action of specimens, mainly including improving the ductility and increasing the interlayer displacement angle.

Table 5 Performance indexes of SRHSC short-limb shear walls from references

Reference	Mean μ	Code	Good use		Ensuring the personal safety		Preventing the collapse	
			Δ_1 (mm)	θ_1	Δ_2 (mm)	θ_2	Δ_3 (mm)	θ_3
Xie (2008)	3.43	SW-1	3.93	1/379	16.68	1/89	26.59	1/56
	3.32	SW-3	3.66	1/407	19.25	1/77	23.00	1/65
Yu (2009)	3.77	SW-1	1.20	1/1250	11.00	1/136	20.58	1/73
	3.92	SW-2	1.40	1/1071	14.74	1/102	23.70	1/63
	4.73	SW-3	1.40	1/1071	14.23	1/105	26.95	1/56
	4.32	SW-4	1.50	1/1000	13.60	1/110	25.53	1/59
Li (2010)	5.03	SW-1	1.70	1/882	16.41	1/91	27.46	1/55
	-	SW-2	1.70	1/882	19.18	1/78	22.00	1/68
	3.64	SW-3	1.60	1/938	16.44	1/91	21.97	1/68
Wang (2008)	6.05	JG500	3.91	1/332	62.52	1/21	81.20	1/16
	5.12	JG550	1.27	1/1024	40.19	1/32	55.40	1/24
	4.83	JG600	1.05	1/1238	39.20	1/33	50.20	1/26
Yang *et al*. (2009)	4.67	CSW-5	1.73	1/751	45.25	1/29	58.63	1/22
	4.20	CSW-5.5	1.64	1/795	34.91	1/37	44.70	1/29
	5.40	CSW-6	1.78	1/732	46.04	1/28	55.60	1/23

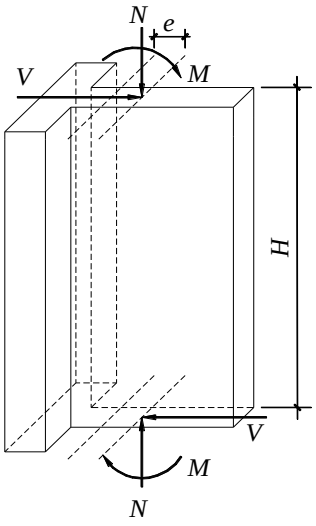

Fig. 15 Simplified force model

4. Shear capacity of SHSRCSLSW

4.1 Cracking strength

According to the experimental observation, the flexural cracks occurred for all the specimens in the initial loading, so sectional analysis method can be used to calculate the concrete cracking strength. Fig. 15 shows the force model of shear wall under the complex stress state of pressure, bending, shear and so on. Here it can be assumed that before the specimen cracks, the whole body of SRHSC short-limb shear wall is in the elastic stress state. When the concrete cracks at the root of wall limbs, there were horizontal flexural crack. Hence, the maximum tensile stress $\sigma_{\max}$ in the cracking zone reaches the concrete tensile strength f_t

$$\sigma_{\max} = \frac{M}{W} - \frac{N}{A} = f_{\mathrm{t}} \tag{3}$$

$$M = VH + Ne \tag{4}$$

In this investigation, there are two differences need to be reconsidered for T-shaped SRHSC short-limb shear walls. One is the irregularity of cross section characterized by T-shaped form; the other is the high strength concrete material compared with normal concrete. Therefore, the shear wall bending section coefficient or cross-sectional inertia moment can be complex. The equivalence principle is always used in the engineering calculation for its simplifying the calculation procedure. Based on the above idea, the transformed section method is used to simplify the calculation, and two assumptions are put forward to support this method as follows: 1) the vertical load is applied in the web center of T-shaped cross section; 2) both areas of shape steel and reinforcement bars are equivalent to the concrete area, and the calculated neutral axis gets through the centroid of T-shaped cross section, however, for the small ratio of wall limb height to thickness, the neutral axis should be moved from the section centroid to the flange side and its

distance from the centroid should be determined by calculation. The converted concrete section area A and converted inertia moment I_0 are shown as follows.

$$A = A_c + \alpha_{ss} A_{ss} + \alpha_s A_s \tag{5}$$

$$I_o = I_c + \alpha_{ss} I_{ss} + \alpha_s I_s \tag{6}$$

Where A_c, A_{ss} and A_s are the cross-sectional areas of concrete, shape steel and reinforcement bar, respectively. I_c, I_{ss} and I_s are the cross sectional inertia moments of net concrete, shape steel and reinforcement bar, respectively. α_{ss} is the ratio of shape steel elasticity modulus to concrete elasticity modulus; α_s is the ratio of reinforcement bar elasticity modulus to concrete elasticity modulus. The concrete elasticity modulus E_c can be obtained from Chinese standard GB500010-2010.

Through integrating Eq. (3) and Eq. (4), the cracking capacity of T-shaped SHSRCSLSW can be obtained as

$$V_{cr} = \left(f_t + \frac{N}{A} \right) \frac{W}{H} - \frac{Ne}{H} \tag{7}$$

Where W is the shear wall bending section coefficient after conversion; N is the axial compressive load; A is the shear wall concrete cross section area after conversion; H is the length of specimen; e is the distance of vertical load point to sectional centroid of converted concrete cross section.

Table 6 lists the calculation results of cracking capacity of all the specimens. After comparison, it can be found that the average ratio of test results to calculation values is 1.06, the standard deviation of these ratios is 0.231 and the coefficient of variation of these ratios is 0.218, indicating that the theoretical calculation by using the equivalence principle can agree well with the test results.

4.2 Shear strength

In this study, the major destruction of T-shaped SRHSC short-limb shear wall specimens was the shear-diagonal compressive failure, which emerged in the web direction with crushing the concrete into rhombus blocks. When the specimens were destroyed, both strains of web member (or steel flat) of shape steel and stirrup were reaching the yielding point. In order to simplify the calculation, the bond action between shape steel and concrete need to be neglected, so that they are the part of independent. Hence, the shear strength of shear wall can be evaluated using the superposition method. As the name implies, the shear strengths contributed by the concrete, the steel and the reinforcement stirrup are calculated separately. As a result, the shear capacity of T-shaped SRHSC short-limb shear wall (V) can be expressed as

$$V = V_s + V_{rc} \tag{8}$$

Where V_s is the shear strength of shape steel, V_{rc} is the shear strength of RC.

For the specimens configured with truss typed steel, as suggested by Xue *et al*. (2012), the shear strength contributed by oblique and horizontal steel flats is similar to that contributed by reinforcement stirrup. Here, according to the theory of reinforced concrete structures (GB50010-2010), the diagonal web member and horizontal web member can be regarded as

bend-up reinforcement bar and stirrup, respectively.

$$V_s = f_{sw} A_w \cos\alpha + \frac{A_{wh}}{s_w} f_{sw} h_0 \tag{9}$$

Where f_{sw} is the yield strength of steel web member; A_w is the cross-sectional area of oblique steel web member, α is the dip angle of oblique steel flat to horizontal steel flat paralleling to the shear force direction; A_{wh} is the cross-sectional area of horizontal steel web member, s_w is the separation distance of contiguous horizontal steel web members up and down, h_0=h-a_{ss} is the calculated or effective height of horizontal steel web member, a_{ss} is the concrete protective covering thickness of longitudinal shape steel.

For the part of RC, the shear capacity of reinforced concrete mainly includes the capacities of concrete and stirrup contributed, and meanwhile, the axial pressure should also be considered to affect the shear strength of component. As suggested by Xue *et al*. (2012), Yang *et al*. (2010), Zhou *et al*. (2012), there are significant effects of wall flange and strength grade of high strength concrete on the shear capacity of T-shaped SRHSC short-limb shear wall, so that these effects need to be reflected in the theoretical calculation model. Based on the previous research on RC special shaped columns (JGJ149-2006), the RC shear strength of T-shaped SRHSC short-limb shear wall induced by seism is calculated as Eq. (10). In addition, as suggested by CECS10:499 (1999) the structural concrete strength should be reduced as the concrete design strength grade exceeds 50 MPa.

$$V_{rc} = \frac{1}{\gamma_{RE}} \left(\frac{1.05}{\lambda + 1.0} \xi_f \alpha_c f_t b_c h_0 + \frac{A_{sv}}{s_{sv}} f_{sv} h_0 + 0.056N \right) \tag{10}$$

$$\alpha_c = \sqrt{23.5 / f_c} \tag{11}$$

Where γ_{RE} is the seismic adjustment coefficient of shear capacity, and it can be set the value as 0.85. When λ<1.0, λ=1.0; When λ>3.0, λ=3.0. ξ_f is the flange influence coefficient, here it can be set the value as 1.083 (Xue *et al*. 2012). f_{sv} is the yield strength of stirrup. A_{sv}=nA_{sv1} is the total area of all stirrups configured in the wall limb which is parallel to the load direction. A_{sv1} is the cross-sectional area of single limb stirrup, n is the number of stirrup limbs within the same cross section. s_{sv} is the separation distance of contiguous stirrups in the cross section of wall limb

Table 6 Predictions of concrete cracking strength and ultimate shear strength of specimens

Specimen code	N (kN)	e (mm)	V_c^t (kN)	V_c^c (kN)	V_c^t / V_c^c	V_u^t (kN)	V_u^c (kN)	V_u^t / V_u^c
TW-1	730	53.3	40	38.0	**1.05**	460.6	468.5	**0.98**
TW-2	810	53.3	60	59.8	**1.00**	546.0	457.4	**1.19**
TW-3	931	61.0	90	88.4	**1.02**	634.9	617.6	**1.03**
TW-4	1424	61.0	130	112.7	**1.15**	590.9	650.7	**0.91**
TW-5	1075	117.0	30	41.7	**0.72**	694.8	769.5	**0.90**
TW-6	1094	117.0	60	41.9	**1.43**	736.5	853.9	**0.86**

Note: N is the axial compressive force; V_c^t is the concrete cracking capacity by test; V_c^c is the concrete cracking capacity by calculation; V_u^t is the shear capacity by test; V_u^c is the shear capacity by calculation.

paralleling to the load direction. b_c is the cross-sectional width of wall limb paralleling to the load direction. $h_0=h-a_s$ is the effective height of wall limb cross section paralleling to the load direction, and a_s is concrete protective covering thickness of longitudinal reinforcement bar. When $N \geq 0.3(f_cA_c+f_sA_{ss})$, N is equal to $0.3(f_cA_c+f_sA_{ss})$. a_c is the strength reduction coefficient of high strength concrete.

Table 6 lists the calculation results of shear capacity of all the specimens. After comparison, it can be found that the average ratio of test results to calculation values is 0.98, the standard deviation of these ratios is 0.121 and the coefficient of variation of these ratios is 0.123, indicating that the calculation values by using the superposition principle can agree well with the test results.

5. Conclusions

This paper presents an experimental and analytical study on the cyclic behavior of T-shaped steel reinforced high strength concrete short-limb shear wall configured with T-shaped steel truss.

(1) In the experimental program, the structural mechanisms and failure modes of the shear wall were intensively investigated as follows:

- Two main failures were obtained for T-shaped SRHSC short-limb shear walls, including the flexural failure with large shear/span ratio and shear-diagonal compressive failure with small shear/span ratio.
- The specimen flexural failure exhibited which had lower loading capacity and stiffness, but higher energy dissipation capacity and better ductility than that with shear-diagonal compressive failure.
- An increase of axial compression ratio leads to an increase of positive peak loading capacity, initial elastic lateral stiffness and energy dissipation capacity, but a decrease of negative peak loading capacity, elastic-plastic lateral stiffness and deformation capacity.
- The effect of stirrup reinforcement ratio on the stiffness of specimens illustrates that there is no significant difference in the early stage of loading, however, the elastic-plastic lateral stiffness for the short-limb shear wall member can be enhanced due to the increasing of stirrup reinforcement ratio. In addition, the specimen with large stirrup reinforcement ratio demonstrates higher loading capacity, stiffness and ductility, but lower cumulative energy dissipation capacity than that with small stirrup reinforcement ratio.
- When the wall limb height to thickness ratio is at the value of 6.5, the cumulative energy dissipation capacities of specimens are larger than those of the specimens with the ratios of 5 and 8. Furthermore, an increase of wall limb height to thickness ratio leads to significant reduction of ductility.
- Measures such as setting constraints at the end of component limb, increasing stirrup ratio in the cross section, setting oblique supports and optimizing steel configuration form were put forward to enhance the seismic action of T-shaped SRHSC short-limb shear walls, for the deformation capacity of test specimens could not meet the level of ‘three’ fortification goals compared with the steel reinforced normal strength concrete short-limb shear wall.

(2) In the analytical research, the mechanical analysis models for concrete cracking strength and shear strength are derived using the equivalence principle and superposition theory, respectively. As a result, the proposed method in this paper is verified by the test results, and the experimental values agree well with the calculation values.

Acknowledgements

The authors would like to thank the Natural Science Foundation of China (No. 50908057 and 51268004), the Open Project of Guangxi Key Laboratory of Disaster Prevention and Structural Safety (No: 2012ZDX10 and 2014ZDK0011) and Project of Guangxi Graduate Education Innovation Program (No: YCBZ2012005). The founding and support from the above projects are greatly acknowledged.

References

Altin, S., Anil, Ö., Kopraman, Y. and Kara, M.E. (2013), "Hysteretic behavior of RC shear walls strengthened with CFRP strips", *Compos. Part B*, **44**, 321-329.

Altin, S., Kopraman, Y. and Baran, M. (2013), "Strengthening of RC walls using externally bonding of steel strips", *Eng. Struct*., **49**, 686-695.

Brueggen, B.L. (2009), "Performance of T-shaped reinforced concrete structural walls under multi-directional loading", University of Minnesota, Minneapolis.

China Association for Engineering Construction Standardization, CECS10:499 (1999), *Technical specification for high-strength concrete structures*, China Plan Press, Beijing. (in Chinese)

China Construction Department, GB50010-2010 (2010), *Code for design of concrete structures*, China Construction Industry Press, Beijing. (in Chinese)

China Construction Department, GB50011-2010 (2010), *Code for seismic design of buildings*, *China Construction Industry Press*, Beijing. (in Chinese)

China Construction Department, JGJ149-2006 (2006), *Technical specification for concrete structures with specially shaped columns*, China Construction Industry Press, Beijing. (in Chinese)

China Construction Department, JGJ3-2010 (2011), *Technical specification for concrete structures of tall building*, China Construction Industry Press, Beijing. (in Chinese)

Dai, K. (2013), "Breakthrough of traditional shear wall structure system-short-leg wall structure system", *Struct. Des. Tall Spec. Build.*, **22**(16), 1270-1278.

Ding, J.G. and Zhu, Y. (2012), "An elastic-plastic analysis of short-leg shear wall structures during earthquakes", *Earthq. Eng. Eng. Vib.*, **11**(4), 525-540.

Gonzales, H. and López-Almansa, F. (2012), "Seismic performance of buildings with thin RC bearing walls", *Eng. Struct.*, **34**, 244-258.

Jalali, A. and Dashti, F. (2010), "Nonlinear behavior of reinforced concrete shear walls using macroscopic and microscopic models", *Eng. Struct.*, **32**(9), 2959-2968.

Lao, X.C. and Han, X.L. (2011), "Performance index limits of high reinforced concrete shear wall components", *J. Cent. South Univ. Technol*., **18**(4), 1248-1255.

Li, Q.J. (2010), "Study on a new short shear wall structure set the core steel tube concrete column", MS Thesis, Guangxi University, Nanning, China. (in Chinese)

Li, W. and Li, Q.N. (2012), "Seismic performance of L-shaped RC shear wall subjected to cyclic loading", *Struct. Des. Tall Spec. Build.*, **21**(12), 855-866.

Liao, F.Y., Han, L.H. and Tao, Z. (2012), "Performance of reinforced concrete shear walls with steel reinforced concrete boundary columns", *Eng. Struct.*, **44**, 186-209.

Meftah, S.A. and Tounsi, A. (2007), "Lateral stiffness and vibration characteristics of damaged RC coupled shear walls strengthened with thin composite plates", *Build. Environ.*, **42**(10), 3596-3605.

Mosoarca, M. (2013), "Seismic behaviour of reinforced concrete shear walls with regular and staggered openings after the strong earthquakes between 2009 and 2011", *Eng. Fail. Anal.*, **34**, 537-565.

Mosoarca, M. (2014), "Failure analysis of RC shear walls with staggered openings under seismic loads", *Eng. Fail. Anal.*, **41**, 48-64.

Mullapudi, T.R.S., Charkhchi, P. and Ayoub, A. (2013), "Behavior of shear-dominant thin-walled RC structures", *Thin Wall. Struct.*, **63**, 134-146.

Nie, J.G., Hu, H.S., Fan, J.S., Tao, M.X., Li, S.Y. and Liu, F.J. (2013), "Experimental study on seismic behavior of high-strength concrete filled double-steel-plate composite walls", *J. Constr. Steel Res.*, **88**, 206-219.

Qian, J.R., Jiang, Z. and Ji, X.D. (2012), "Behavior of steel tube-reinforced concrete composite walls subjected to high axial force and cyclic loading", *Eng. Struct.*, **36**, 173-184.

Quiroz, L.G., Maruyama, Y. and Zavala, C. (2013), "Cyclic behavior of thin RC Peruvian shear walls: Full-scale experimental investigation and numerical simulation", *Eng. Struct.*, **52**, 153-167.

Rong, B.S. (1997), "Short-leg shear wall structural system used in tall residential building", *J. Build. Struct.*, **18**(6), 14-19. (in Chinese)

Su, R.K.L. and Wong, S.M. (2007), "Seismic behaviour of slender reinforced concrete shear walls under high axial load ratio", *Eng. Struct.*, **29**(8), 1957-1965.

Tao, M.X., Fan, J.S. and Nie, J.G. (2013), "Seismic behavior of steel reinforced concrete column-steel truss beam hybrid joints", *Eng. Struct.*, **56**, 1557-1569.

Wang, X.Y. (2008), "Experimental on seismic performance of steel-concrete composion short pier shear wall", MS Thesis, Beijing University of Technology, Beijing, China. (in Chinese)

Xie, H. (2008), "The experimental study on antiseismic behavior of short shear wall which adopts prestressed concrete and shape steel concrete", MS Thesis, Guangxi University, Nanning, China. (in Chinese)

Xue, J.Y., Chen, Z.P., Zhao, H.T., Gao, L. and Liu, Z.Q. (2012), "Shear mechanism and bearing capacity calculation on steel reinforced concrete special-shaped columns", *Steel Compo. Struct*., **13**(5), 473-487.

Xue, LM. (2005), "Nonlinear finite element analysis of mechanical performance of reinforced concrete short-limb shear wall", *Wuhan Univ. J. Nat. Sci.*, **10**(3), 562-565.

Yamada, M. (1992), "Steel panel encased RC composite shear wall", *Composite Construction in Steel and Concrete II*, ASCE, 899-912.

Yang, Q., Fan, Y., Wang, X. and Zheng, L. (2009), "Experimental studies on seismic behavior of shape steel concrete short-leg shear walls", *World Earthq. Eng.*, **25**(2), 105-110. (in Chinese)

Yang, Y.L., Yang, H. and Zhang, S.M. (2010), "Compressive behavior of T-shaped concrete filled steel tubular columns", *Int. J. Steel Struct.*,**10**(4), 419-430.

Yu, L. (2009), "The experimental study on antiseismic behavior of the new steel-concrete composite short pier shear wall of restricted type", MS Thesis, Guangxi University, Nanning, China. (in Chinese)

Zhang, Q., Tao, C.C., Wei, C.B., Zhuang, J., Tan, P. and Liang, Y.H. (2011), "The elastic-plasticity analysis on cross-section short-limb shear wall", *Advanced Materials Research, 2011 International Conference on Structures and Building Materials*, ICSBM, **163-167**, 913-917.

Zhou, H.Y., Attard, T.L., Zhao, B., Yu, J.T., Lu, W.S. and Tong, L.W. (2013), "Experimental study of retrofitted reinforced concrete shear wall and concrete-encased steel girders using a new Carbon Flex composite for damage stabilization", *Eng. Fail. Anal.*, **35**, 219-233.

Zhou, T., Chen, Z.H. and Liu, H.B. (2012), "Seismic behavior of special shaped column composed of concrete filled steel tubes", *J. Constr. Steel Res.*, **75**, 131-141.

CC